

Influence of ZrB₂ Content on the Oxidation Behavior of Nb-Mo-ZrB₂ Composites

Gao Yuan, Liu Zongde, Wang Qi, Sun Youmei, Gong Yan

Key Laboratory of Condition Monitoring and Control for Power Plant Equipment of Ministry of Education, North China Electric Power University, Beijing 102206, China

Abstract: The NbMo solid solution (denoted as (Nb, Mo)ss hereinafter) matrix ceramic composites reinforced with 15 vol%, 30 vol%, 45 vol%, and 60 vol% ZrB₂ particles were fabricated by hot-pressing sintering at 2400 °C. The effect of the ZrB₂ content on the isothermal oxidation resistance and the oxide scales microstructure evolution at 800, 1000, and 1200 °C was investigated. The results show that both temperature and ZrB₂ content have an influence on the oxidation behavior. The oxidation resistance of ZrB₂-(Nb, Mo)ss composites increases with increasing ZrB₂ content and decreases with increasing oxidation temperature from the view point of parabolic rate constant. The oxide scales at 800~1000 °C contain special film-like Nb₂Zr₆O₁₇, acting as a barrier against oxygen diffusing inwards and leading to low parabolic rate constant. However, no Nb₂Zr₆O₁₇ layer is observed at 1200 °C because the volatile MoO₃ and the volume effect of ZrO₂ damage the Nb₂Zr₆O₁₇ protective layer which results in severe spallation and poor oxidation resistance. Possible oxidation mechanisms at different temperatures with varying ZrB₂ contents were discussed according to the observed oxide morphologies and the results above.

Key words: metal matrix ceramic composites; ZrB₂; oxidation behavior

Niobium-based alloys are attractive as one of the most promising refractory metals for space, nuclear and aircraft^[1-3] in terms of their low density, good ductility and high melting point. However, the use of niobium-based alloys is restricted by the poor oxidation resistance and the low high-temperature strength^[4-6]. The strength of niobium decreases substantially above 900 °C^[4] and “pest oxidation” occurs above 600 °C. As a result, various approaches have been utilized to improve its oxidation resistance and strength including solid solution strengthening^[7,8], composite strengthening with intermetallic compounds such as Nb₃Al, Nb₃Ir and Nb₅Si₃^[9,10], and composite strengthening using carbide phase^[11-13]. In the previous work^[13], it is found that adding Mo into niobium-based alloy can form NbMo solid solution and improve the yield strength. The maximum solid solution effects can be achieved when the Nb/Mo atom ratio is around 1. It is also proved that adding Mo into Nb can reduce the solubility of oxygen in niobium-based alloy and improve oxidation

resistance. Tan et al^[4] observed that the introduction of ceramic particle second phase such as ZrC, can improve high temperature strength and oxidation resistance of niobium-based composites.

Zirconium diboride has received much attention because it offers low density (6.09 g/cm³), high melting point (3040 °C) and good thermal shock resistance^[14,15]. The oxidation of ZrB₂ or ZrB₂-based composites, such as ZrB₂-SiC, leads to the formation of crystalline ZrO₂, liquid B₂O₃ and silicate glass. Amorphous boron oxide or silicate glass on the exposed surfaces can protect the substrate from oxidation^[16]. Therefore, ZrB₂ based materials possess excellent oxidation resistance^[17]. However, few studies have focused on NbMo solid solution matrix composites reinforced with ZrB₂ particles.

In order to increase high temperature strength and oxidation resistance of niobium-based composite, NbMo solid solution matrix composite reinforced with ZrB₂ particles were fabricated by hot-pressing sintering in our previous work^[18,19].

Received date: December 18, 2018

Foundation item: National Natural Science Foundation of China (11372110)

Corresponding author: Liu Zongde, Ph. D., Professor, Key Laboratory of Condition Monitoring and Control for Power Plant Equipment of Ministry of Education, North China Electric Power University, Beijing 102206, P. R. China, E-mail: lzd@ncepu.edu.cn

Copyright © 2019, Northwest Institute for Nonferrous Metal Research. Published by Science Press. All rights reserved.

The results showed that ZrB₂-(Nb, Mo)ss composite exhibited excellent mechanical properties. Its highest room temperature strength reached 1635.91 MPa and the high temperature strength was also excellent^[19]. However, the effect of the ZrB₂ content on the isothermal oxidation resistance of ZrB₂-(Nb, Mo)ss composites have not been clarified yet.

In the present paper, isothermal oxidation behavior of (0 vol%~60 vol%)ZrB₂-(Nb, Mo)ss at 800, 1000 and 1200 °C was investigated. The oxidation kinetic curves were acquired, and the phase constitution and microstructure evolution were also analyzed and the influence of ZrB₂ content on oxidation mechanisms was also discussed in detail.

1 Experiment

The (0 vol%~60 vol%)ZrB₂-(Nb, Mo)ss composites were prepared by hot-pressing sintering according to the nominal composition given in Table 1. In the present paper, all the composition will be given in volume fraction unless specially emphasized. Commercially available ZrB₂ (23 μm, purity>99.9%), Nb and Mo (18~25 μm, purity>99.95%) were supplied by Beijing Gold Crown New Material Technology Co. Ltd, China. A two-step fabrication schedule including powder compaction process^[20] and high temperature sintering was used based on 2400 °C sintering temperature and 35 MPa uniaxial pressure. The details were shown in Ref. [18]. The specimens of 0 vol%, 15 vol%, 30 vol%, 45 vol%, and 60 vol%ZrB₂-(Nb, Mo)ss were denoted as NM, NM-15Z, NM-30Z, NM-45Z, NM-60Z, respectively.

Isothermal oxidation tests were conducted at 800, 1000, and 1200 °C using a zirconia tube furnace (SK-6, Fuensen furnace Co. Ltd, Beijing, China). The oxidized samples were weighed using a Mettler Toledo balance with a sensitivity of 0.0001 g. A Rigaku D/max-rA X-ray diffractometer with Cu Kα radiation, between 2θ angles of 10° and 90° at a scanning rate of 8°/min was used to identify the main phases. Morphology studies were performed using scanning electron microscopes (FEI Quanta 200F) equipped with an EDAX genesis xm-2 X-ray spectrometer (EDS).

2 Results

2.1 Microstructure before oxidation test

In our previous work, the relationship between microstructure and mechanical properties of ZrB₂-(Nb, Mo)ss composites were investigated^[18,19]. As already reported before^[19], the main phases of ZrB₂-(Nb, Mo)ss composites consist of NbMo solid solution and ZrB_x particles including

ZrB₂ and ZrB. The influence on the oxidation behavior of other phases such as Nb₃B₂, NbB, and Mo₂Zr can be neglected because the quality of them is small. Fig.1 shows the SEM images of the polished surface of the hot-pressed ZrB₂-(Nb, Mo)ss composites before oxidation test. As the arrow pointed out, the dark gray area is Nb-rich (Nb, Mo)ss and the light gray area is the Mo-rich (Nb, Mo)ss^[18]. It should be noted that the shape of Nb-rich (Nb, Mo)ss changes from irregular shape to dendrites shape and the Mo-rich (Nb, Mo)ss and the round ZrB_x phases tend to distribute around the dendrites when ZrB₂ content increases from 15 vol% to 60 vol%. As shown in Fig.1, the location of ZrB_x can be divided into two types. In NM-15Z, most ZrB_x particles distribute in the Mo-rich (Nb, Mo)ss while in NM-30Z, NM-45Z and NM-60Z, ZrB_x particles distribute along with Nb-rich (Nb, Mo)ss. This phenomenon has a great influence on the oxidation behavior and the reasons will be discussed in the following sections.

2.2 Oxidation kinetic curves from 800 °C to 1200 °C

Fig.2~4 shows typical isothermal oxidation kinetic curves of the ZrB₂-(Nb, Mo)ss composites oxidized at 800, 1000 and 1200 °C for 40 h. The kinetics curves change from linear law to parabolic characteristic when ZrB₂ content exceeds 45%. The relationship between mass gain and oxidation time can be expressed as^[21-23]:

$$\Delta w = k_p t^n \quad (1)$$

where, Δw is the mass gain per unit area ($\text{mg}\cdot\text{cm}^{-2}$), k_p is the oxidation rate constant ($\text{mg}\cdot\text{cm}^{-2}\cdot\text{h}^{-n}$), t is the oxidation time (h) and n is the time exponent that describes the time dependence of oxide growth. NM, NM-15Z and NM-30Z expand a lot after several hours of oxidation because of poor oxidation resistance resulting in interruption of oxidation test. The time exponents of ZrB₂-(Nb, Mo)ss composites fitted based on Eq. (1) are shown in Table 2. The parabolic law assumes the transport of either vacancies or interstitials of ions through a uniform oxide film. In fact, many defects (pores, cracks, and grain boundaries) exist in the real oxide films that may affect the effective diffusivity, resulting in a deviation in the time exponent from the parabolic law ($n=0.5$)^[24]. In the study of the oxidation behavior of ferritic-martensitic steel in supercritical water reported by Zhu before^[25], the time exponent for P92 samples exposed to SCW at different temperatures changes from 0.42 to 0.47. However, the actual oxidation kinetics that P92 samples followed is parabolic law. As shown in Table 2, it can be reasonably speculated that a parabolic time dependence of the mass gain is followed by NM-30Z at 800 °C, by NM-45Z and NM-60Z at both 800 and 1000 °C. The kinetic curves exhibit linear characteristics ($n=1$) for NM at all three different temperatures. A transition from parabolic law to linear law is observed in NM-15Z and NM-30Z at both 1000 and 1200 °C and in NM-60Z at 1200 °C. These findings suggest that both oxidation temperature and ZrB₂ content have an influence on the oxidation behavior.

The fitted linear equations between the mass gain (Δw) and

Table 1 Nominal composition of ZrB₂-(Nb, Mo)ss composites (vol%)

Sample	NM	NM-15Z	NM-30Z	NM-45Z	NM-60Z
Nb	50	42.5	35	27.5	20
Mo	50	42.5	35	27.5	20
ZrB ₂	0	15	30	45	60

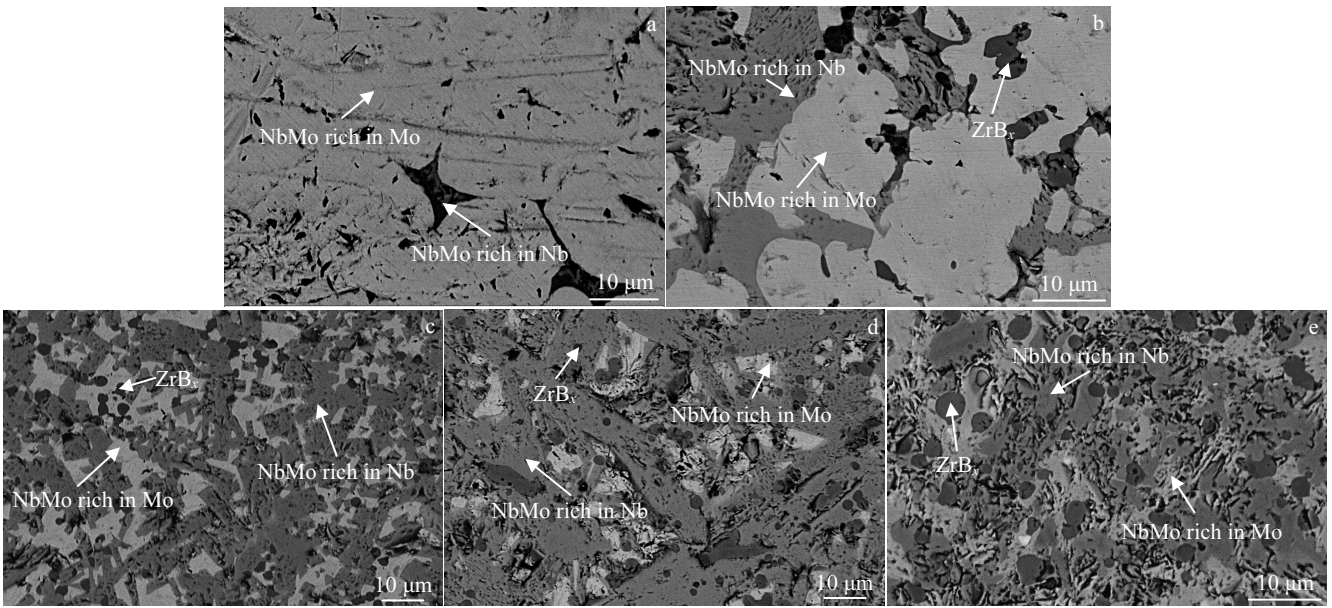


Fig.1 SEM back-scattered electron images before oxidation test: (a) NM, (b) NM-15Z, (c) NM-30Z, (d) NM-45Z, and (e) NM-60Z

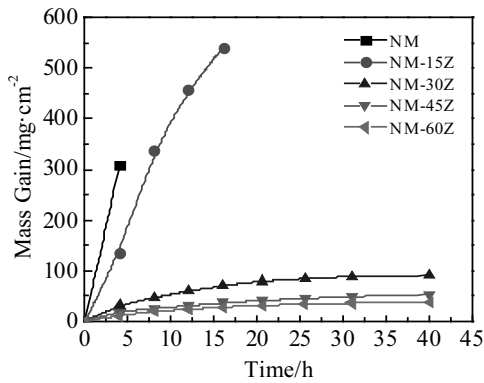


Fig.2 Oxidation kinetic curves of ZrB₂-(Nb, Mo)ss composites exposed at 800 °C for 40 h in static air

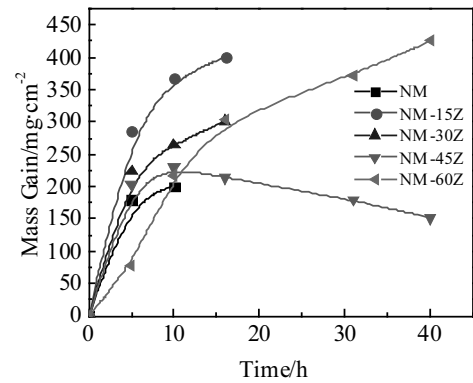


Fig.4 Oxidation kinetic curves of ZrB₂-(Nb, Mo)ss composites exposed at 1200 °C for 40 h in static air

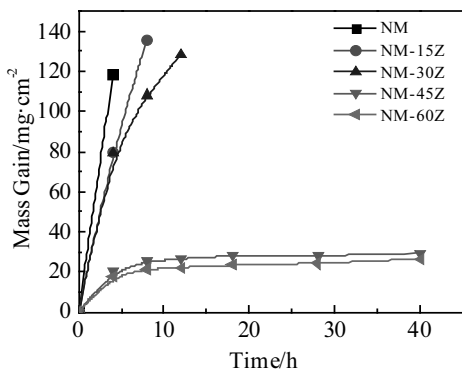


Fig.3 Oxidation kinetic curves of ZrB₂-(Nb, Mo)ss composites exposed at 1000 °C for 40 h in static air

Table 2 Time exponent (*n*) of ZrB₂-(Nb, Mo)ss composites from 800 °C to 1200 °C

Sample	NM	NM-15Z	NM-30Z	NM-45Z	NM-60Z
800 °C	1	1	0.44	0.47	0.47
1000 °C	1	0.77	0.73	0.41	0.42
1200 °C	1	0.79	0.69	-	0.72

the square root of the oxidation time ($t^{0.5}$), and the corresponding parabolic rate constant k_p ($\text{mg}^2 \cdot \text{cm}^{-4} \cdot \text{h}^{-1}$), considering the parabolic formula of $\Delta w^2 = k_p t^{126}$) are shown in Table 3. The data of the other composites (not mentioned in Table 3 as compared with Table 2) are not calculated because the kinetics curve of them exhibits linear characteristics or a transition from parabolic to linear characteristics rather than parabolic characteristics. The k_p of NM-60Z is lower than those of other

Table 3 Fitted linear equations and parabolic rate constant k_p values ($\text{mg}^2\cdot\text{cm}^{-4}\cdot\text{h}^{-1}$) for the oxidation of ZrB_2 - $(\text{Nb}, \text{Mo})\text{ss}$ composites from 800 °C to 1000 °C

Sample (temperature)	Equation	R^2	k_p
NM-30Z (800 °C)	$y=11.86x^{0.5}$	0.9589	3.44
NM-45Z (800 °C)	$y=6.45x^{0.5}$	0.9367	2.54
NM-60Z (800 °C)	$y=4.77x^{0.5}$	0.9441	2.18
NM-45Z (1000 °C)	$y=5.26x^{0.5}$	0.9739	2.29
NM-60Z (1000 °C)	$y=4.55x^{0.5}$	0.9614	2.13

investigated composites, by approximately 14%–37% at 800 °C, and by 7% at 1000 °C, demonstrating that the higher the ZrB_2 content, the better the oxidation resistance from the viewpoint of parabolic rate constant k_p .

2.3 Phases of the oxides from 800 °C to 1200 °C

Fig.5 shows the XRD patterns of oxidation products of NM and NM-60Z. As indicated by Fig.5a, the oxide scales of NM from 800 °C to 1200 °C contain NbO_2 , Nb_2O_5 and MoO_3 . The oxidation products of NM-15Z, NM-30Z, NM-45Z is similar to those of NM-60Z. As shown in Fig.5b, oxidation products of NM-60Z at 800 and 1000 °C include B_2O_3 , NbO_2 , Nb_2O_5 , MoO_3 , ZrO_2 and $\text{Nb}_2\text{Zr}_6\text{O}_{17}$. However, the B_2O_3 phase cannot be detected at 1200 °C in NM-60Z.

NbO_2 and Nb_2O_5 were previously observed for the oxidation of niobium alloyed^[27]. The formation of ZrO_2 and B_2O_3

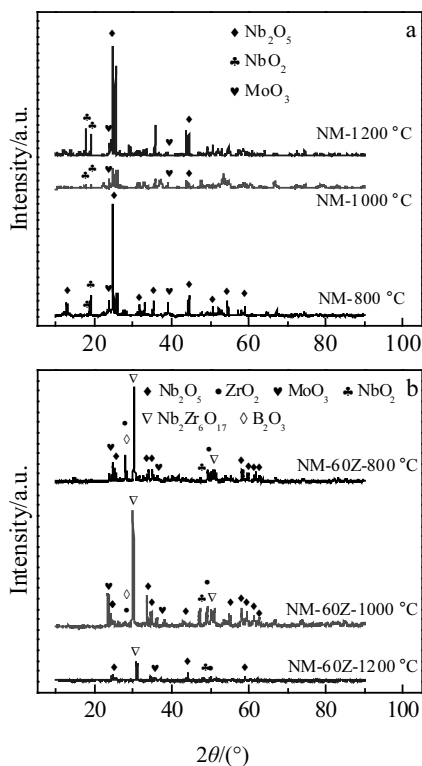


Fig.5 XRD patterns of the corrosion products of NM (a) and NM-60Z (b)

are due to the oxidation of ZrB_x distributed in the NbMo solid solution matrix. As reported by several researchers before^[28-30], the oxidation of ZrB_2 results in two phases ZrO_2 and B_2O_3 , and the distribution of the phases in the scale varies with temperature. At lower temperatures (≤ 1000 °C), a glassy B_2O_3 film is observed on top of the ($\text{ZrO}_2+\text{B}_2\text{O}_3$) scale, while this external boric layer is absent at higher temperatures (1200 °C) because of the evaporation of B_2O_3 . As a result, no B_2O_3 phase is detected after oxidation test at 1200 °C in this paper. Minor peaks of MoO_3 are also identified. In general, Mo is usually oxidized selectively and preferentially to form MoO_3 due to lower oxygen partial pressure in those alloys or compounds containing Mo^[31,32] and the MoO_3 starts vaporizing above 500 °C^[33]. In this paper, MoO_3 was also vaporized during high temperature oxidation and then deposited on the surface of oxide scales during cooling. The white powders on the surface of the oxide scale (Fig.12) can be regarded as the evidence of the existence of MoO_3 . The peaks corresponding to $\text{Nb}_2\text{Zr}_6\text{O}_{17}$ phase are also detected and its formation results from the simultaneous oxidation of niobium and zirconium diborides. According to the phase diagram^[34] presented in Fig.6, Nb_2O_5 can react with ZrO_2 to form $\text{Nb}_2\text{Zr}_6\text{O}_{17}$, as demonstrated in Eq. (2):



2.4 Morphologies of the oxides from 800 °C to 1200 °C

The oxidation products of NM from 800 °C to 1200 °C are similar so that morphology at 800 °C is displayed as a representation. As shown in Fig.7a and Table 4, it can be concluded that the lath-like phase is Nb_2O_5 . The broken bubbles at the lath-like phase may be caused by the volatility of MoO_3 ^[15,16,35]. MoO_3 are known to adversely affect the densification of the oxide scale and they usually degrade the oxidation resistance in those alloys or compounds containing Mo^[32,33].

The morphology of oxidation products of ZrB_2 - $(\text{Nb}, \text{Mo})\text{ss}$ composites with varying ZrB_2 contents exposed at 800 °C for

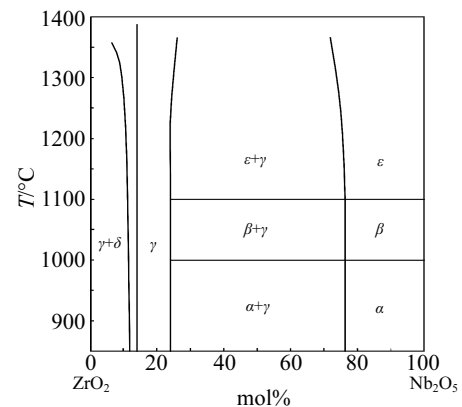


Fig.6 Phase diagram for Nb_2O_5 - ZrO_2 ^[34] (α =orthorhombic Nb_2O_5 , β =monoclinic Nb_2O_5 , ε =orthorhombic Nb_2O_5 , γ = $\text{Nb}_2\text{Zr}_6\text{O}_{17}$, δ =monoclinic ZrO_2)

40 h is shown in Fig.7b~7e. It can be seen that the oxidation of niobium results in evaporation-resistant refractory oxide Nb_2O_5 that forms a porous skeleton^[36] and the growth of lath-like Nb_2O_5 is restricted by a film-like phase observed in NM-45Z and NM-60Z. According to the EDS results in Table 5 and XRD analysis in Fig.5, it can be concluded that the film-like phase is $\text{Nb}_2\text{Zr}_6\text{O}_{17}$. The film-like $\text{Nb}_2\text{Zr}_6\text{O}_{17}$ covered at Nb_2O_5 can heal the interspaces between Nb_2O_5 to inhibit the diffusion of oxygen into the inner part of the composites. As a result, more $\text{Nb}_2\text{Zr}_6\text{O}_{17}$ forms resulting in the better oxidation resistance of ZrB_2 -(Nb, Mo)ss composites. This result is in accordance with the oxidation kinetic curves.

Fig.8 illustrates the morphology of oxidation products of ZrB_2 -(Nb, Mo)ss composites with varying ZrB_2 contents exposed at 1000 °C for 40 h. It can be seen that a lot of holes and interspace are observed in NM-15Z and NM-30Z which provide diffusion channels for oxygen to further oxidation. However, the cracks and holes are healed by film-like $\text{Nb}_2\text{Zr}_6\text{O}_{17}$ in NM-45Z and NM-60Z. The holes in NM-30Z are speculated to be caused by the volatility of MoO_3 because

the location of holes are in accordance with Mo-rich (Nb, Mo)ss as shown in Fig.1c. As illustrated in Fig.8, it can be observed that the amount of $\text{Nb}_2\text{Zr}_6\text{O}_{17}$ increases with increasing ZrB_2 content. Only a few $\text{Nb}_2\text{Zr}_6\text{O}_{17}$ form in NM-15Z and NM-30Z resulting in a lot of unhealed holes. However, with increasing ZrB_2 content up to 45 vol% and 60 vol%, the film-like $\text{Nb}_2\text{Zr}_6\text{O}_{17}$ can cover the surface of the cracks and holes acting as a barrier against oxygen diffusing inwards. The morphology of oxidation products of NM-45Z and NM-60Z exposed at 1000 °C is in good agreement with the oxidation kinetics curves obtained in 1000 °C which also indicates that the higher ZrB_2 content in ZrB_2 -(Nb, Mo)ss composites results better oxidation resistance.

The morphology of oxidation products of ZrB_2 -(Nb, Mo)ss composites with varying ZrB_2 contents exposed at 1200 °C for 40 h is shown in Fig.9. The lath-like Nb_2O_5 and the holes existed in NM-15Z and NM-30Z after oxidized at 1200 °C are very similar to those observed at 800 and 1000 °C. The most difference in the morphology is that no obvious film-like $\text{Nb}_2\text{Zr}_6\text{O}_{17}$ can be observed after oxidation at 1200 °C in NM-

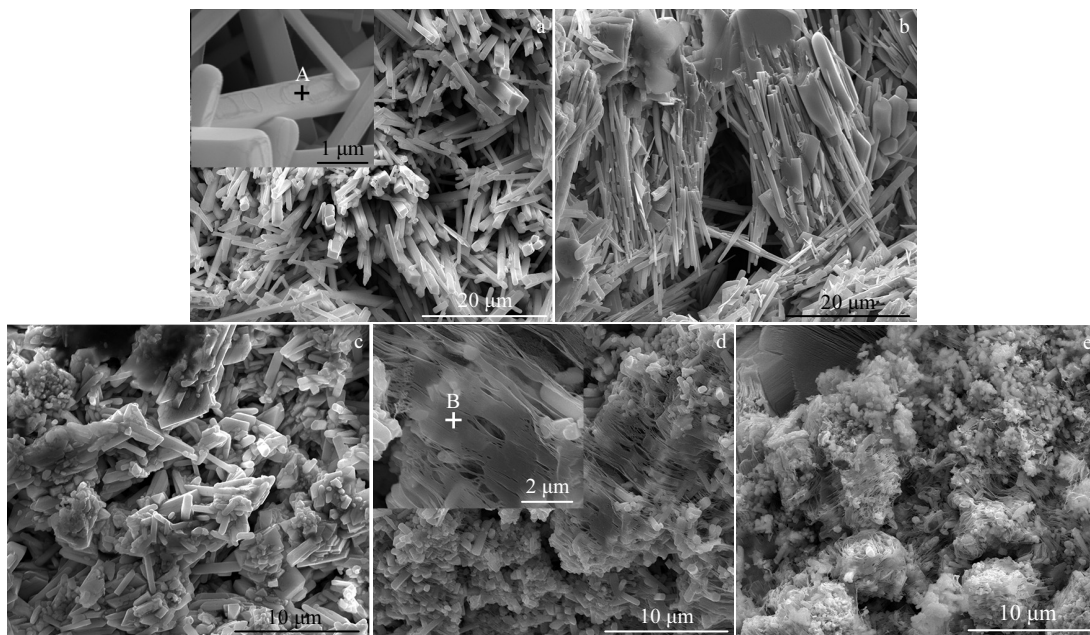


Fig.7 SEM secondary electron images of the cross-section morphology of NM (a), NM-15Z (b), NM-30Z (c), NM-45Z (d), and NM-60Z (e) exposed at 800 °C for 40 h

Table 4 EDS results of spot A in Fig.7a

Element	O K	Nb L	Mo L
wt%	24.83	57.21	12.08
at%	65.82	26.12	5.66

Table 5 EDS results of spot B in Fig.7d

Element	O K	Zr L	Nb L	Mo L
wt%	26.49	41.54	31.97	0.00
at%	67.43	18.55	14.02	0.00

45Z and NM-60Z. As reported by Xiao et al^[36], MoO_3 evaporates severely above 1155 °C. As a result, the vaporization of MoO_3 may damage the $\text{Nb}_2\text{Zr}_6\text{O}_{17}$ layer during oxidation test. This phenomenon is also observed in the study of oxidation behavior of novel Co-Al-W-Ta-B-(Mo, Hf, Nb) alloys which found that the vaporization of MoO_3 may damage or remove the continuous Al_2O_3 layer formed earlier. Without the protection of $\text{Nb}_2\text{Zr}_6\text{O}_{17}$, the oxidation resistance of NM-45Z and NM-60Z decreases and the oxidation kinetics

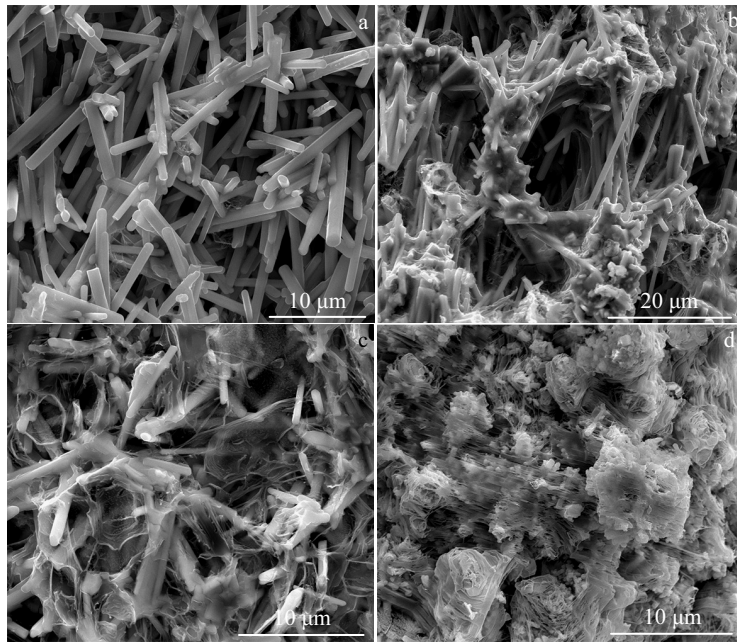


Fig.8 SEM secondary electron images of the cross-section morphology of NM-15Z (a), NM-30Z (b), NM-45Z (c), and NM-60Z (d) exposed at 1000 °C for 40 h

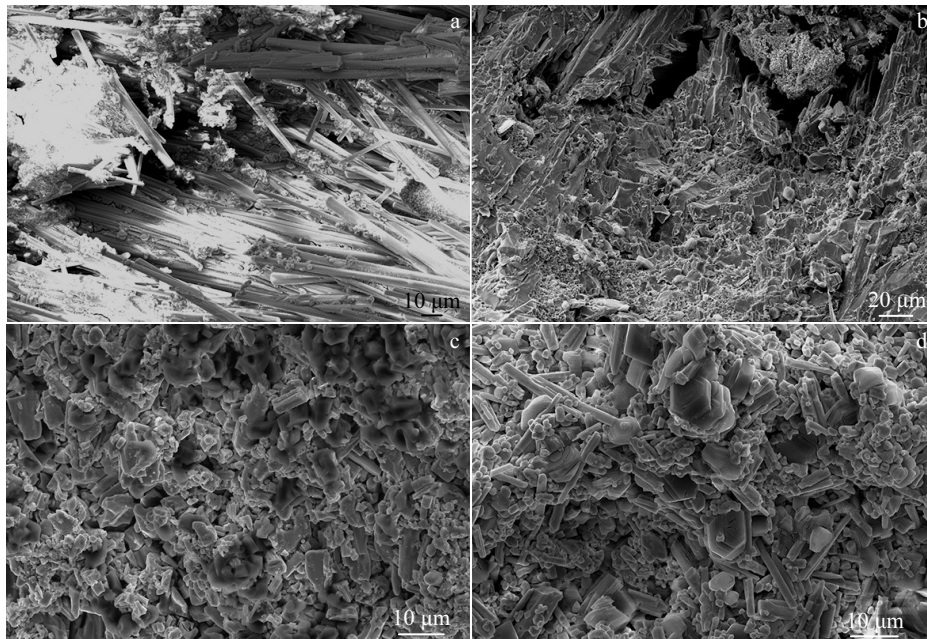


Fig.9 SEM secondary electron images of the cross-section morphology of NM-15Z (a), NM-30Z (b), NM-45Z (c), and NM-60Z (d) exposed at 1200 °C for 40 h

curves show a transition from parabolic characteristic to linear characteristic as displayed in Fig.4. In addition, the shape of ZrO_2 changes from dense cuboid in Fig.10a to polyhedron with many cracks on the surface in Fig.10b. The cracks are demonstrated to be caused by volume effect during crystal

transition^[37] and also act as the diffusion channels for oxygen diffusing towards the substrate.

3 Discussion

The data in Table 2 and 3 suggests that the oxidation

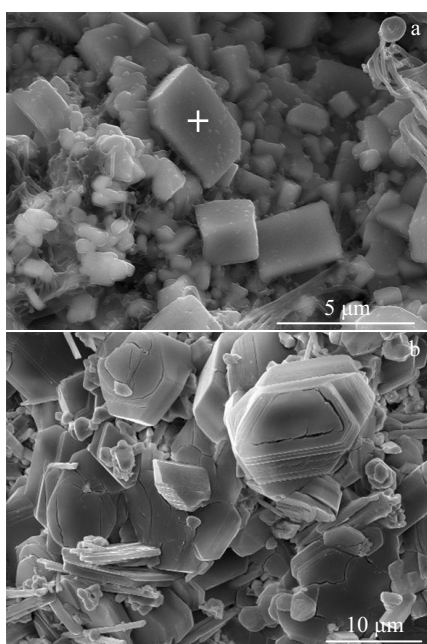


Fig.10 SEM secondary electron images of ZrO_2 formed at different temperatures: (a) 1000 °C and (b) 1200 °C

resistance of ZrB_2 -(Nb, Mo)ss composites is related to the ZrB_2 content. The NM-60Z with the highest ZrB_2 content 60 vol% gets the lowest parabolic rate constant at 800 °C ($2.18 \text{ mg}^2\cdot\text{cm}^{-4}\cdot\text{h}^{-1}$) and 1000 °C ($2.13 \text{ mg}^2\cdot\text{cm}^{-4}\cdot\text{h}^{-1}$). The good oxidation resistance is mainly due to the formation of $Nb_2Zr_6O_{17}$ protective layer acting as a barrier against oxygen diffusing inwards. However, when the ZrB_2 content is lower than 45%, such as 30% and 15% in this paper, the completed $Nb_2Zr_6O_{17}$ protective layer cannot be formed and oxidation kinetics curves show the linear or near-linear characteristic indicating poor oxidation resistance. Apparently, the oxidation

resistance of ZrB_2 -(Nb, Mo)ss composites increases with increasing ZrB_2 content.

In addition, the temperature also has an influence on the oxidation resistance and the oxides microstructure, especially in NM-45Z and NM-60Z. To better understand the oxidation step, the cross-section SEM images and elemental distribution of the oxide scale of NM-60Z at 1000 °C are shown in Fig.11. The oxygen content decreasing to nearly zero from the external layer to substrates indicates that the oxygen diffusion is restricted after the initial oxidation at the surface. The Mo content increases to the maximum value at the substrate/oxide interfaces but decreases apparently at the oxide scales, suggesting that MoO_3 volatilizes at the external layer and that Mo diffuses from substrate to surface during oxidation process. At the beginning of oxidation process, the diffusion of the Mo from inner part to the surface leads to the formation of MoO_3 and Nb is oxidized into Nb_2O_5 at the same time. The volatility of MoO_3 provides diffusion channels for oxygen diffusing inwards to further react with ZrB_2 particles to form B_2O_3 and ZrO_2 . Then, the formed ZrO_2 reacts with Nb_2O_5 to form $Nb_2Zr_6O_{17}$. As presented in Fig.7 and 8, film-like $Nb_2Zr_6O_{17}$ can heal the cracks caused by the volatility of MoO_3 , restrict the diffusion of oxygen and inhibit the free growth of Nb_2O_5 . The diffusion of both oxygen and metal ion changes into diffusion of metal ion. As a result, the oxidation rate reduces and the oxidation kinetics displays a near-parabolic law as shown in Fig.2 and 3.

In addition, the film-like $Nb_2Zr_6O_{17}$ covered on the surface of Nb_2O_5 inhibits the oxygen diffusion and reduces the oxygen partial pressure resulting in the formation of sub-oxide NbO_2 (Fig.5). As reported before, the pilling-bedworth ratio (PBR) of Nb_2O_5 (2.74) is high enough to make the oxide scale separate from the substrate^[38]. When the free growth of Nb_2O_5 is restricted, the inner stress of oxide scales is reduced, and the oxidation layer becomes adherent to substrate.

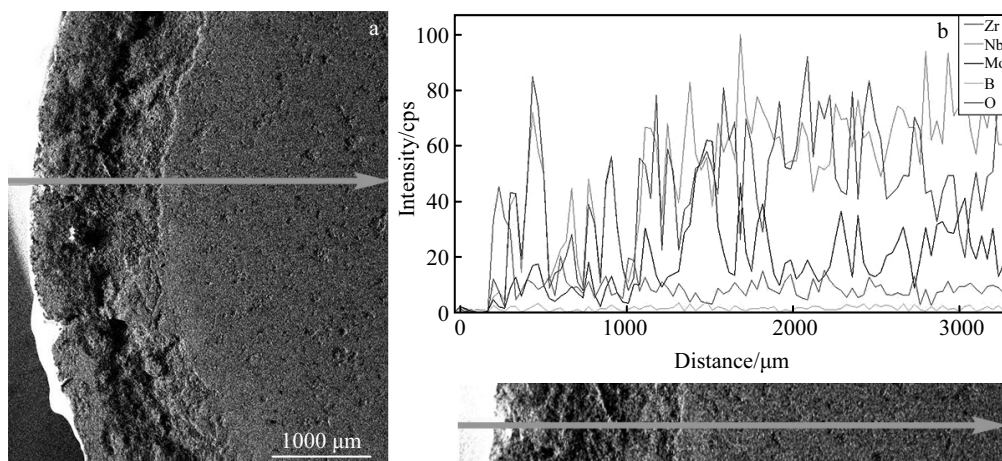


Fig.11 SEM secondary electron image (a) and elemental distribution (b) of the oxide scales of NM-60Z exposed at 1000 °C for 40 h

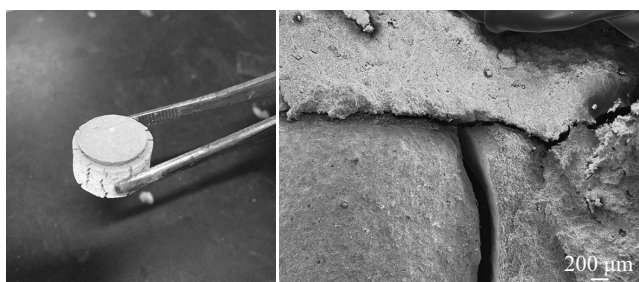


Fig.12 Micro-morphology of NM-60Z exposed at 1200 °C for 40 h

The oxidation resistance and oxides microstructure of NM-45Z and NM-60Z at 1200 °C are different compared to those at 800~1000 °C which is mainly due to the severe evaporation of MoO₃ above 1155 °C^[36]. As reported before, during the period of increasing temperature, the MoO₃ oxide forms and its vapor pressure rises sharply from 10⁻² Pa to 10² Pa as temperature increases up to 1000 °C^[33]. This suggests that an increasing temperature enhances the vaporizing rate of MoO₃. MoO₃ may damage the Nb₂Zr₆O₁₇ layer and the cracks and pores caused by the evaporation of MoO₃ provide more rapid diffusion channels for oxygen and enhance oxidation, which may be the reason why the NM-45Z and NM-60Z exhibit poor oxidation resistance at 1200 °C. As reported by previous study^[39], the ZrO₂ can recrystallize into a dense coherent subscale, which can protect the underlying ceramics from catastrophic oxidation. However, in this work, the cracks on the ZrO₂ grains caused by volume effect also provide rapid diffusion channels for oxygen and degrade the oxidation resistance of ZrB₂-NbMo composites at 1200 °C. When cooled down from 1200 °C to room temperature, the crystal structure of ZrO₂ changed from the tetragonal (t-ZrO₂, space group P4₂/nmc) to highly distorted monoclinic (m-ZrO₂, space group P2₁/c) with 5%~7% volume expansion^[37] and generated the inner stress of oxidation layers. As a result, the cracks could be observed on the surface of ZrO₂ and the oxide scales tended to spall off from the substrate as shown in Fig.12. The spallation of oxide scales makes the substrate to be exposed in air and also degrades the oxidation resistance.

4 Conclusions

1) The oxidation resistance of ZrB₂-(Nb, Mo)ss increases with increasing ZrB₂ content. The kinetics curves change from linear law to parabolic characteristic when ZrB₂ content exceeds 45% at 800~1000 °C.

2) The oxidation of (45~60 vol%)ZrB₂-(Nb, Mo)ss at 800~1000 °C leads to the formation of film-like Nb₂Zr₆O₁₇ which can heal the cracks caused by the evaporation of MoO₃ and protect the substrate from further oxidation.

3) The volume effect of ZrO₂ and the severe evaporation of MoO₃ weaken the adhesion of the oxide scale, enhance the

exfoliation of the oxide products and damage the protective Nb₂Zr₆O₁₇ layer, resulting in severe spallation and poor oxidation resistance of ZrB₂-(Nb, Mo)ss at 1200 °C.

References

- Silvestroni L, Meriggi G, Sciti D. *Corrosion Science*[J], 2014, 83: 281
- Fahrenholtz W G, Hilmas G E, Talmy I G et al. *Journal of the American Ceramic Society*[J], 2007, 90(5): 1347
- Zhang X J, He X D, Fan C L et al. *International Journal of Refractory Metals and Hard Materials*[J], 2013, 41: 185
- Tan Y, Ma C L, Kasama A et al. *Materials Science and Engineering A*[J], 2003, 355: 260
- Yan J J, Guo X P. *Rare Metal Materials and Engineering*[J], 2017, 46(1): 1
- Sun Z P, Guo J M, Zhang C et al. *Rare Metal Materials and Engineering*[J], 2016, 45(7): 1678
- Kasimtssev A V, Yudin S N, Logacheva A I et al. *Inorganic Materials*[J], 2015, 51(1): 43
- Guo Y L, Jia L L, Kong B et al. *Journal of Alloy and Compounds*[J], 2017, 696: 516
- Sun Z P, Guo X P, Tian X D et al. *Rare Metal Materials and Engineering*[J], 2015, 44(9): 2148
- Duan Y H. *Rare Metal Materials and Engineering*[J], 2015, 44(1): 18
- Wei B X, Wang Y J, Zhao Y W et al. *International Journal of Refractory Metals and Hard Materials*[J], 2018, 70: 66
- Mannan P, Casillas G, Pereloma E V. *Materials Science and Engineering A*[J], 2017, 700: 116
- Tan Y, Ma C L, Kasama A et al. *Materials Science and Engineering A*[J], 2003, 341: 282
- Chamberlain A L, Fahrenholtz W G, Hilmas G E. *Journal of the American Ceramic Society*[J], 2006, 89(2): 450
- Song J G, Luo H M, Du D M et al. *Materials Review*[J], 2009, 23(2): 43 (in Chinese)
- Gao D, Zhang Y, Xu CL et al. *Journal of Inorganic Materials*[J], 2011, 26(4): 434 (in Chinese)
- Zhang LY, Fei T, Zeng W Y et al. *Corrosion Science*[J], 2015, 100: 421
- Gao Y, Liu Z D, Wang Q et al. *International Journal of Minerals, Metallurgy and Materials*[J], 2018, 25(7): 824
- Liu Z D, Wang Q, Gao Y et al. *International Journal of Refractory Metals and Hard Materials*[J], 2017, 68: 104
- Saxena A, Singh N, Kumar D et al. *Materials Today: Proceedings*[J], 2017, 4: 5561
- Ampornrat P, Was G S. *Journal of Nuclear Materials*[J], 2007, 371: 1
- Zhong X Y, Wu X Q, Han E H. *Corrosion Science*[J], 2015, 90: 511
- Yin K, Qiu S, Tang R et al. *Journal of Supercritical Fluids*[J], 2009, 50: 235
- Zhu Z L, Xu H, Jiang D F et al. *Oxidation of Metals*[J], 2016, 86: 483

- 25 Zhu Z L, Xu H, Jiang D F et al. *Corrosion Science*[J], 2016, 113: 172
- 26 He J B, Wang Y G, Luo L et al. *Journal of the European Ceramic Society*[J], 2016, 36: 3769
- 27 Li T F. *Oxidation and Corrosion of Metals at High Temperature, 2nd ed*[M]. Beijing: Chemistry Industry Press, 2003: 235 (in Chinese)
- 28 Parthasarathy T A, Rapp R A, Opeka M et al. *Acta Materialia*[J], 2007, 55: 5999
- 29 Opeka M M, Talmy I G, Zaykoski J A. *Journal of Materials Science*[J], 2004, 39: 5887
- 30 Wuchina E, Opeka M, Causey S et al. *Journal of Materials Science*[J], 2004, 39: 5939
- 31 Zhu R Z, He Y D, Qi H B et al. *High-Temperature Corrosion and Materials of High-temperature Resistance*[M]. Shanghai: Shanghai Science and Technology Press, 1995: 465 (in Chinese)
- 32 Wang B, Sun C, Gong J et al. *Surface and Coatings Technology*[J], 2002, 149: 70
- 33 Samant M S, Kerkar A S, Bharadwaj S R et al. *Journal of Alloy and Compounds*[J], 1992, 187: 373
- 34 Massalski T B. *Binary Alloy Phase Diagram*[M]. Ohio: American Society for Metals, 1986: 746
- 35 Wang C, Liang J, Luan X et al. *Rare Metal Materials and Engineering*[J], 2009, 38(S2): 886 (in Chinese)
- 36 Xiao L R, Yao B, Pei X Y et al. *Ordinance Material Science and Engineering*[J], 2015, 38(6): 27 (in Chinese)
- 37 Chen L T. *Thesis for Master*[D]. Wuhan: Wuhan University of Technology, 2008
- 38 Birks N, Meier G H, Pettit F S. *Introduction to the High Temperature Oxidation of Metals*[M]. Cambridge: Cambridge University Press, 2006: 668
- 39 Han J C, Hu P, Zhang X H et al. *Composites Science and Technology*[J], 2008, 68(3-4): 799

ZrB₂含量对 Nb-Mo-ZrB₂复合材料氧化行为的影响

高远, 刘宗德, 王琦, 孙有美, 龚燕

(华北电力大学 电站设备状态监测与控制教育部重点实验室, 北京 102206)

摘要: 利用热压烧结法, 在 2400 °C 烧结温度下, 制备了 NbMo 固溶体 (此后记作(Nb, Mo)ss) 基陶瓷颗粒增强复合材料。其中, ZrB₂ 陶瓷增强相的体积分数分别为 15%, 30%, 45%和 60%。研究了在 800, 1000 和 1200 °C 下, ZrB₂ 含量对复合材料抗氧化性和氧化产物演变的作用。结果表明, 氧化温度和 ZrB₂ 含量均对复合材料的氧化行为有影响。从氧化速率常数角度讲, ZrB₂-(Nb, Mo)ss 复合材料的抗氧化性随 ZrB₂ 含量的增加而提高, 随氧化温度的提高而降低。800~1000 °C 的氧化产物中含有膜状 Nb₂Zr₆O₁₇ 相, 能作为屏障阻止氧气向基体扩散, 因此在 800~1000 °C 时, 复合材料氧化速率较低。然而, 在 1200 °C 氧化时未发现 Nb₂Zr₆O₁₇ 相, MoO₃ 的剧烈挥发和 ZrO₂ 的体积效应破坏了 Nb₂Zr₆O₁₇ 保护层, 导致了氧化层严重剥落, 材料的抗氧化性极差。综上, 结合观察到的氧化产物形貌, 详细阐述了不同 ZrB₂ 含量的复合材料在不同温度下的抗氧化机制。

关键词: 金属基陶瓷复合材料; ZrB₂; 氧化行为

作者简介: 高远, 女, 1993 年生, 博士, 华北电力大学电站设备状态监测与控制教育部重点实验室, 北京 102206, E-mail: 18810178944@163.com